

Earthquake-induced debris flows at Popocatepetl Volcano, Mexico

Velio Coviello¹, Lucia Capra², Gianluca Norini³, Norma Dávila⁴, Dolores Ferrés², Víctor Hugo Márquez-Ramirez², Eduard Pico²

¹ Free University of Bozen-Bolzano, Facoltà di Scienze e Tecnologie, Bolzano, Italy

5 ² Centro de Geociencias, Universidad Nacional Autónoma de México, Campus Juriquilla, Querétaro, México

³ Istituto di Geologia Ambientale e Geoingegneria, Consiglio Nazionale delle Ricerche, Milano, Italy

⁴ Laboratorio de Ciencia y Tecnología de Información Geográfica, Universidad Autónoma del Estado de México, Toluca, México

Correspondence to: Velio Coviello (velio.coviello@unibz.it)

10 **Abstract.** The M7.1 Puebla-Morelos earthquake that occurred on 19 September 2017, with epicenter located ~70 km SW from Popocatepetl volcano, severely hit central Mexico. Seismic shaking of the volcanic edifice induced by the earthquake triggered hundreds of shallow landslides on the ~~volcanic~~ volcano flanks, remobilizing loose pyroclastic deposits and ~~saturated~~ soils saturated by heavy rainfall that occurred between 17th to 19th September 2017. The largest landslides occurred on the slopes of aligned ENE-WSW-trending ravines on opposite sides of the ~~volcanic cone~~, roughly parallel to the regional
15 maximum horizontal stress and local volcanotectonic structural features. This configuration may suggest transient reactivation of local faults and extensional fractures as one of the mechanisms that has weakened the volcanic edifice and promoted the largest slope failures. The seismic records from a broadband station located at few kilometers from the main landslides are used to infer the intensity of ground shaking that triggered the slope failures. The material involved in the larger landslides, mainly ash and pumice fall deposits from late Holocene eruptions with a total volume of about 10⁶ cubic meters, transformed
20 into ~~two-three~~ large debris flows, two on the western slope of the volcano and one on its eastern side. The debris flows were highly viscous and contained abundant large woods (about 10⁵ cubic meter). Their peculiar rheology is reconstructed by field evidences and analyzing the grain size distribution of samples from both landslide ~~sears~~ scarps and deposits. This is the first time that such flows were observed at this volcano. Our work provides new insights to constrain a multi-hazard risk assessment for Popocatepetl and other continental active volcanoes.

25 1 Introduction

Earthquakes can induce large slope instabilities in tectonically active regions, and subsequent rainfall events can dramatically increase the sediment load of the drainage network. Earthquake magnitude (M) and the resulting intensity of ground vibration control the extent of the area where landslides may occur. One of the first comprehensive historical analysis of earthquake-induced landslides was done by Keefer (1984), who showed that the maximum area likely to be affected by landslides during
30 a seismic event increases with M following a power law scaling relationship. In the following years, a growing number of studies started focusing on the impact of landsliding caused by large-magnitude earthquakes on the sediment yield (e.g., Pearce

and Watson, 1986; Dadson et al., 2004; Marc et al., 2019). On active volcanoes, a large variety of factors can promote slope instability and failure such as magma intrusions, hydrothermal activity, gravitational spreading of the basements, climate fluctuations and regional tectonic (Capra et al., 2013; McGuire, 1996; Norini et al., 2008; Roberti et al., 2017; Roverato et al., 2015). In particular, earthquakes are recognized to play one of the most important role in the initiation of slope failures on volcanoes (Kameda et al., 2019; Sassa, 2005; Siebert, 2002). Volcanic slopes that are close to a critical state can be particularly susceptible to perturbations produced by regional earthquakes. Volcanic landslides include a wide spectrum of instability phenomena, from small slope failures to large sector collapse evolving into catastrophic debris avalanches. Intermediate processes such as shallow landslides and debris flows are common in case of an earthquake, but they are relatively poorly documented for past events. Debris flows, often called lahar in volcanic environments, are usually associated with eruptions that induce ice/snow-melt or with intense rainfalls occurring during intra-eruptive phases (e.g., Capra et al., 2018; Major et al., 2016; Manville et al., 2009). Few examples of long-runout debris flows triggered by earthquakes have been described on active volcanoes (Scott et al., 2001). In Mexico, a M6.5 earthquake that occurred in 1920 induced several landslides in the Pico de Orizaba - Cofre de Perote volcanic chain that transformed into debris flows with catastrophic effects for villages along the Huizilapan ravine (Camacho, 1920; Flores, 1922). More recently, several thousands of shallow landslides were triggered by the Tecomán earthquake of 21 January 2003 (M 7.6) in the volcanic highlands north and northwest of Colima City (Keefer et al., 2006). In this paper, we investigate the mass wasting episode triggered by the 19 September 2017, M7.1 Puebla-Morelos earthquake along the eastern and western sides of Popocatepetl volcano. A volume of about 10^6 cubic meters of pre-existing ash and pumice fall deposits ~~have been remobilizedeolapsed~~, producing co-seismic soil slips that transformed into debris flows. This phenomenon, never studied before at Popocatepetl volcano, has important implications for hazard assessment, as the actual hazard map includes only lahars related to volcanic activity (Martin Del Pozzo et al., 2017).

Popocatepetl is one of the most active volcanoes in North America and represents a serious threat for infrastructures and human settlements in central Mexico (Figure 1a). The three major late Holocene eruptions produced pumice fall deposits on the north-east and east sides of the volcano with post-eruptive lahars reaching runout distances up to 50 km in the east and south drainages (Siebe et al., 1996). In recent time, only two large lahar events were observed along the Huiloac Gorge (HG, Figure 1b), in 1997 and 2001, associated with eruptive phases (Capra et al., 2004). Both lahars propagated to the town of Santiago Xalitzinta, 15 km from the volcano's summit (SX, Figure 1b). Apart from the Huiloac Gorge, which was characterized by significant geomorphic transformations due to these latter processes (Tanarro et al., 2010), most drainage network of Popocatepetl volcano has a dense vegetation cover and presents stable, low-energy sediment transport conditions (Castillo et al., 2015). These stable conditions suddenly changed during the M7.1 Puebla-Morelos earthquake when seismic shaking severely hit central Mexico and triggered hundreds of landslides on the slopes of Popocatepetl volcano.

In the following, we provide a general introduction to the geomorphology of Popocatepetl volcano and we shortly describe its recent volcanic activity. Then, we describe the impact of the M7.1 Puebla-Morelos earthquake on the volcano slopes in terms of ground vibrations and landslide activity. Finally, we reconstruct the dynamics of the major landslides and we discuss their transformation into long runout debris flows.

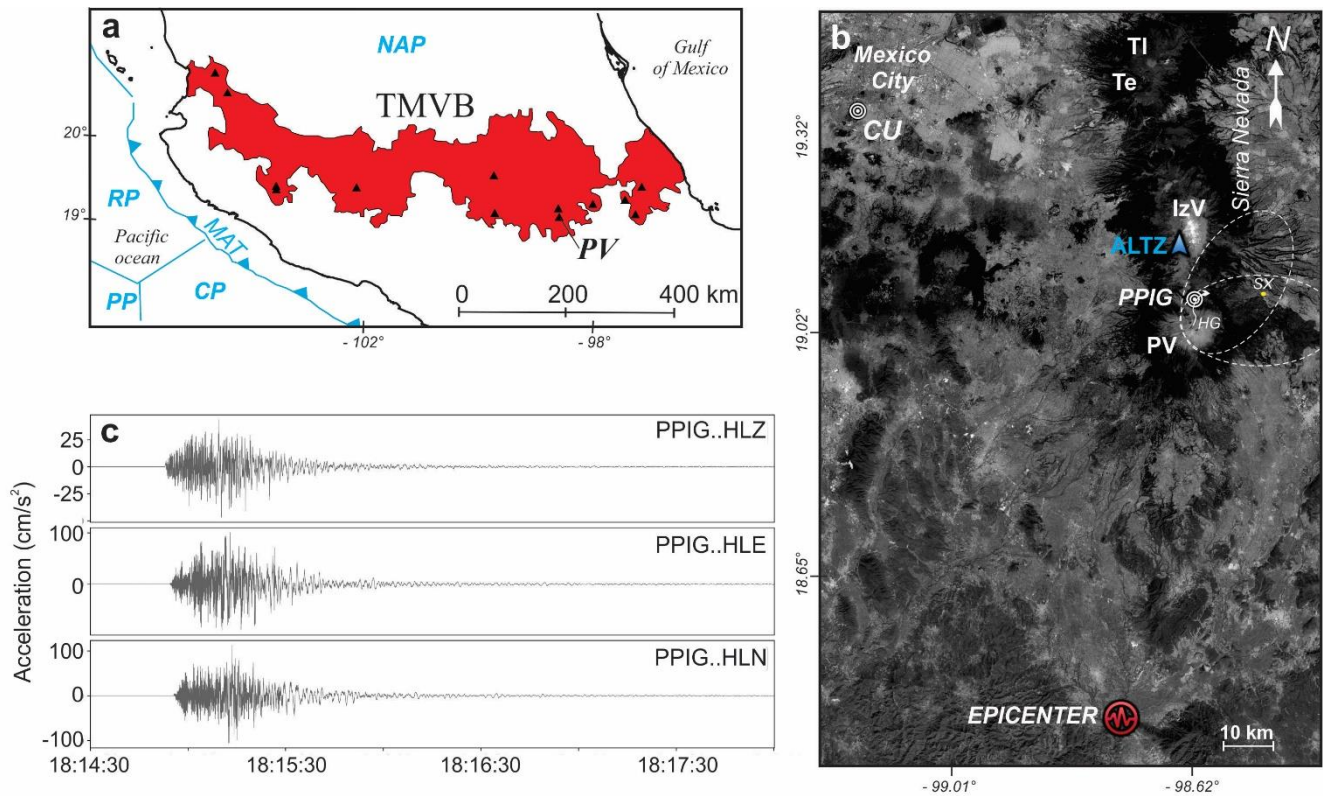


Figure 1: (a) Plate tectonic settings of Central Mexico (CP Cocos Plate, MAT Middle American Trench, NAP North America Plate, PP Pacific Plate) and location of Popocatepetl volcano (PV) in the Trans-Mexican Volcanic Belt (TMVB). (b) Details of the area affected by the M7.1 Puebla-Morelos earthquake and location of the seismic station CU and PPIG and of the rain gauge ALTZ (background image Landsat/Copernicus from Google Earth: ©Google 2020, ©INEGI 2020). (c) Strong motion recorded at station PPIG (SSN-UNAM) during the Puebla-Morelos earthquake on 17 September 2017.

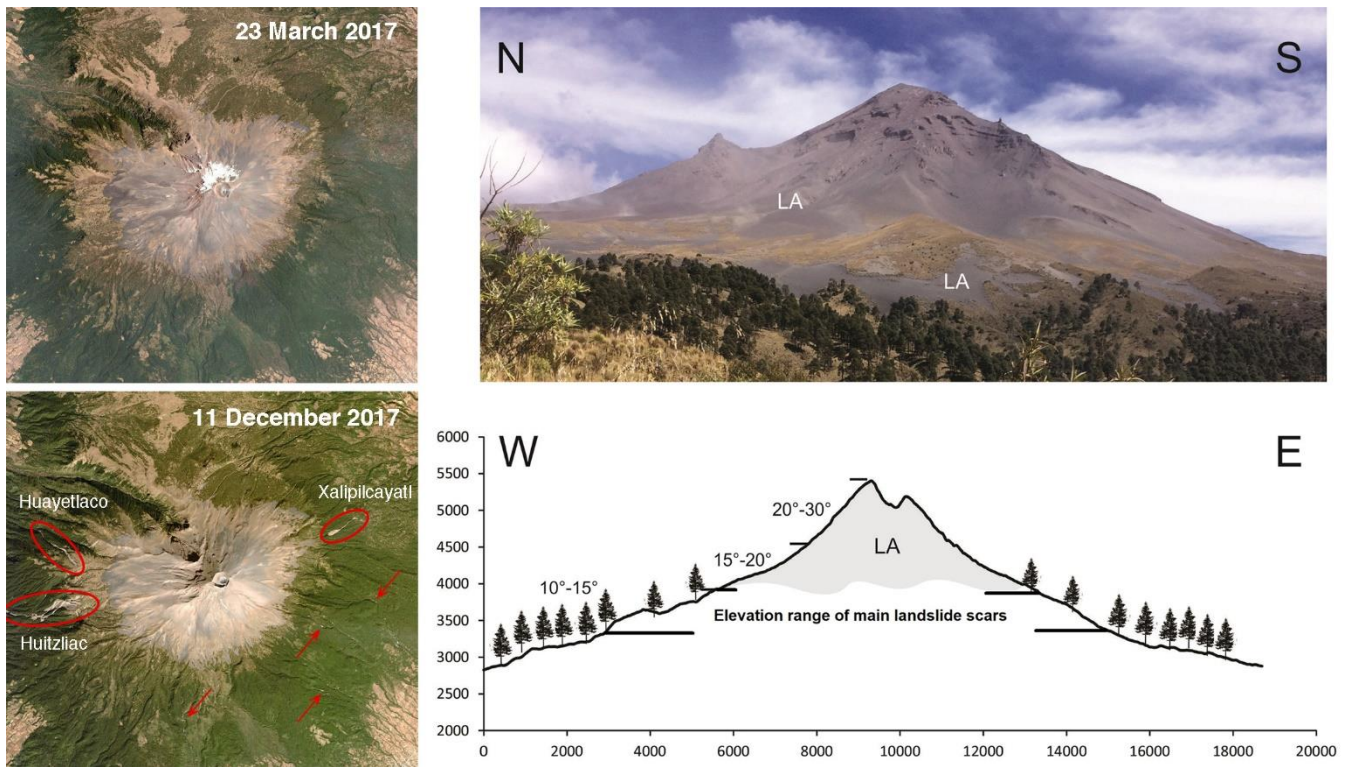
2 Context and study site

On 19 September 2017, central Mexico was hit by a M7.1 intraslab seismic event named Puebla-Morelos earthquake (Melgar et al., 2018). The epicenter of this earthquake is located at a distance of about 70 km SW from the summit of Popocatepetl volcano and of about 100 km SW from Mexico City (Figure 1b). The Puebla-Morelos earthquake produced the most intense ground shaking ever recorded in Mexico City and was the most damaging event for this densely urbanized part of the country since the 1985 M8.1 Michoacán earthquake, that occurred exactly 32 years before (Singh et al., 2018). Several settlements located in the epicentral region were almost completely destroyed. In particular, the earthquake caused severe damage in Mexico City, which is built on a thick clay-rich lacustrine deposit. The damage was surprisingly large in the critical frequency range for Mexico City (0.4–1 Hz), where the earthquake severely damaged hundreds of buildings and killed 369 ~~persons~~ people (Singh et al., 2018). The Peak Ground Acceleration (PGA), calculated as the quadratic mean of the maximum acceleration on the horizontal components, is a standard parameter describing the intensity of strong ground motion during an earthquake.

During the Puebla-Morelos earthquake, the PGA recorded at station Ciudad Universitaria (CU) was the highest recorded in the last 54 years of observations (57.1 cm/s^2) (Singh et al., 2018). Station CU is located on the external boundary of the sedimentary basin responsible for the well-known seismic amplification at Mexico City (Figure 1b). The seismic signal recorded at PPIG station (Figure 1c), located on Popocatepetl volcano slopes at 3980 m a.s.l., featured a much higher value of PGA (158.16 cm/s^2) than the one observed at station CU.

Popocatepetl volcano ($19^\circ 03' \text{N}$, $98^\circ 35' \text{W}$; elevation 5450 m a.s.l.) is located in the central sector of the Trans-Mexican Volcanic Belt (TMVB) (Pasquaré et al., 1987), and it represents the active and southernmost stratovolcano belonging to the Sierra Nevada volcanic chain along with the Telapón-Tlalóc-Iztaccíhuatl volcanoes (Figure 1a-b). The Popocatepetl is a composite ~~cone~~ volcano and; its present shape is the result of eruptive activity that rebuilt the modern cone after the 23.5 ka flank collapse (Siebe et al., 2017). During the Last Glacial Maximum (20-14 ka) the glacier activity resulted in extensive moraines and glacial cirques (Vázquez-Selem and Heine, 2011). Eruptive activity played the primary role in accelerating the glacier retreat on the northern slope of the volcano (Julio-Miranda et al., 2008). The lower part of the cone features a gentle slope ($10\text{-}15^\circ$) and a dense vegetation cover up to approximately 3800 m a.s.l. (Figure 2), where pine trees became scattered and surrounded by dense tropical alpine grasslands (*zacatonal alpino*, Almeida et al., 1994), that can measure up to 1 m in height. Then, the cone becomes progressively steeper ($20\text{-}30^\circ$) and unvegetated up to the summit (Figure 2). In the upper portion of the cone, the slopes are covered by abundant unconsolidated ash named “los arenales” from the recent vulcanian eruptions. The scarps of the main landslides triggered by the 19 September 2017 earthquake generated at elevations of about 3400-3800 m a.s.l. on the internal faces of ravines or glacial cirques where slopes are $> 20^\circ$ (Figure 2).

Historical volcanic activity of Popocatepetl volcano has been characterized by catastrophic episodes including sector collapses and plinian eruptions that emplaced pyroclastic density currents and thick pumice fall deposits, predominantly toward the east (Siebe and Macías, 2006). Based on its Holocene eruptive record, plinian eruptions at Popocatepetl have occurred with variable recurrence time of about 1,000–3,000 years (Siebe et al., 1996). Since 1994, the volcano entered in a new eruptive phase, which includes domes growth that are subsequently destroyed during strong vulcanian eruptions with columns up to 8 km in height, accompanied with ash fall that have been affecting populations in a radius of 100 km approximately. Last major lahars occurred when the Ventorillo glacier was still present on the northern face of the volcano. The 1997 lahar originated after a prolonged explosive activity with emission of ash, which caused the partial melt of the glacier. The rapid release of water gradually eroded the river bed and triggered a debris flow. The 2001 lahar originated from the remobilization of a pumice flow deposit emplaced over the Ventorillo glacier on the northern side of the volcano. The event occurred ~5 hrs after the pyroclastic flow emplacement, and the debris flow was characterized by a stable sediment concentration of 0.75 (Capra et al., 2004). In the distal part, the 1997 lahar transformed into a hyperconcentrated flow, while the 2001 one maintained the characteristics of a debris flow, because of its apparent cohesion due to a silty-rich matrix inherited from the pumice flow deposit.



115

Figure 2: On the left, comparison of optical images of Popocatepetl volcano acquired before and after the earthquake (images ©DigitalGlobe). Earthquake-induced landslides that transformed into debris flows are marked with ellipses. Arrows point at channels punctuated by other small landslides. On the right, NS (picture) and WE (sketch) profiles of the Popocatepetl volcano. LA: Los Arenales.

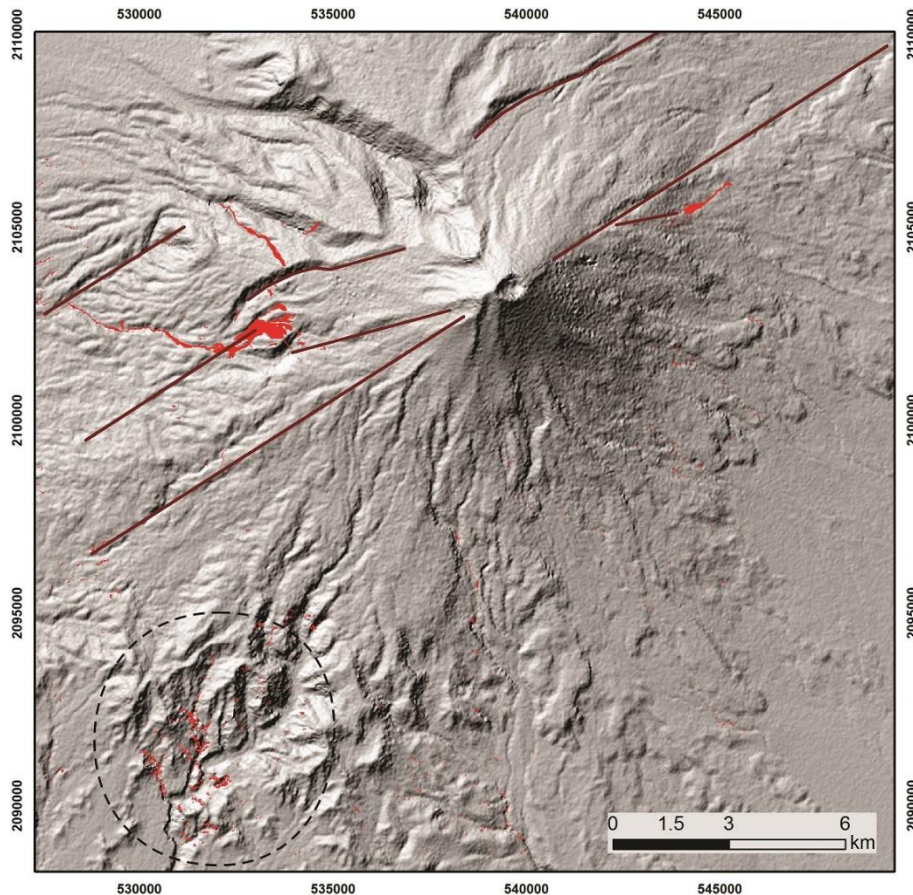
3 Data and methods

120 Satellite data were used to define the extension of the areas affected by landslides and the timing of the landslide occurrences respect to the earthquake event. A preliminary landslide map was constructed based on the interpretation of an archive Pléiades 1A image (incidence angle of 14.63°, resolution of 0.5 m) acquired two months after the earthquake. A Normalized Difference Vegetation Index (NDVI) was calculated using band 1 (red) and band 4 (infrared). The resulting raster was classified for excluding vegetation cover, roads and buildings from the analysis and selecting only landslide scars or depositional areas

125 (Figure 3). We analyzed two Sentinel-1 SAR images (Synthetic Aperture Radar, COPERNICUS program) to define the timing between the earthquake and the observed mass wasting processes. The analyzed images were acquired before and after the earthquake (17 and 23 September 2017) in 1A level Ground Range Detected, ascending orbit, Interferometric Wide sensor mode and dual-polarization. A radiometric calibration was applied to extract the most significant amount of backscattering information from the ground linked to the surficial roughness. As a second step, a change detection technique called Log-Ratio

130 was applied to detect pixel values directly related to radar backscattered correlated to superficial processes; this is an algorithm

used to detect changes using a mean ratio operator between two images of the same area but taken at different times (Mondini, 2017; Singh, 1989).



135 **Figure 3:** Landslide map of the Popocatepetl volcano after the M7.1 Puebla-Morelos earthquake. The polygons corresponding to landslide scars or deposits (red areas) were extracted through the interpretation of a Pléiades 1A image acquired on 13 November 2017. Main volcano-tectonic lineaments are reported (brown lines). The black dashed circle contains the cluster of small soil slips that occurred on the southwestern side of the volcano. Background: 12.5m DEM ©JAXA/METI ALOS PALSAR 2008.

140 Field data were collected from October 2017 to March 2019 to investigate the morphology and stratigraphy of the source area of main landslides, to map and measure faults and fractures caused by the earthquake and to define the extension, thickness and textural characteristics of the larger debris flows (Figure 4). Sampled-Samples were collected on the landslide scars as well as on the debris flow deposits to perform grainsize analysis, by dry-sieving for the sand fraction, and by a laser particle sizer (Analysette 22) for silt and clay fractions.

145 Hydro-metereological~~meteorological~~ data were available from the Alzomoni rain gauge station (ALTZ, RUOA-UNAM, Figure 1b) located at approximately 10 km north from the volcano summit.

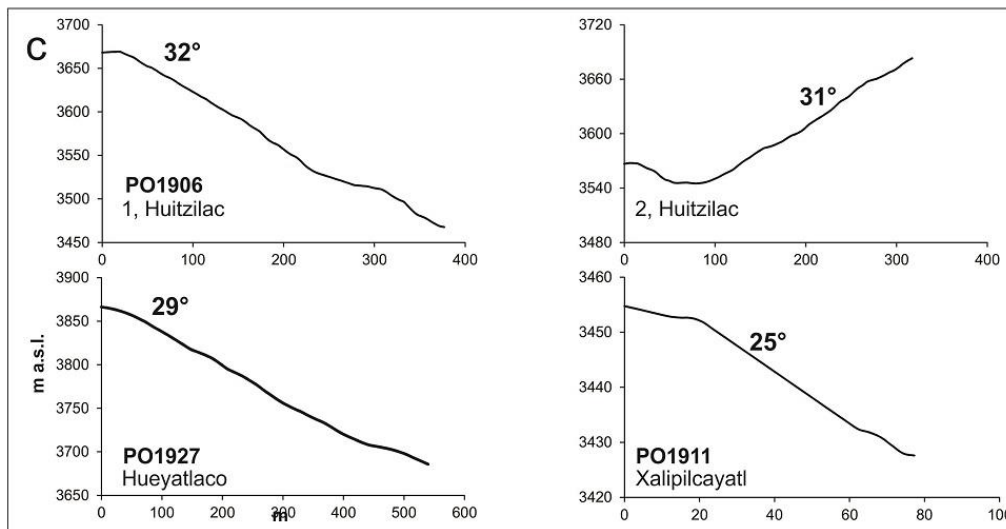
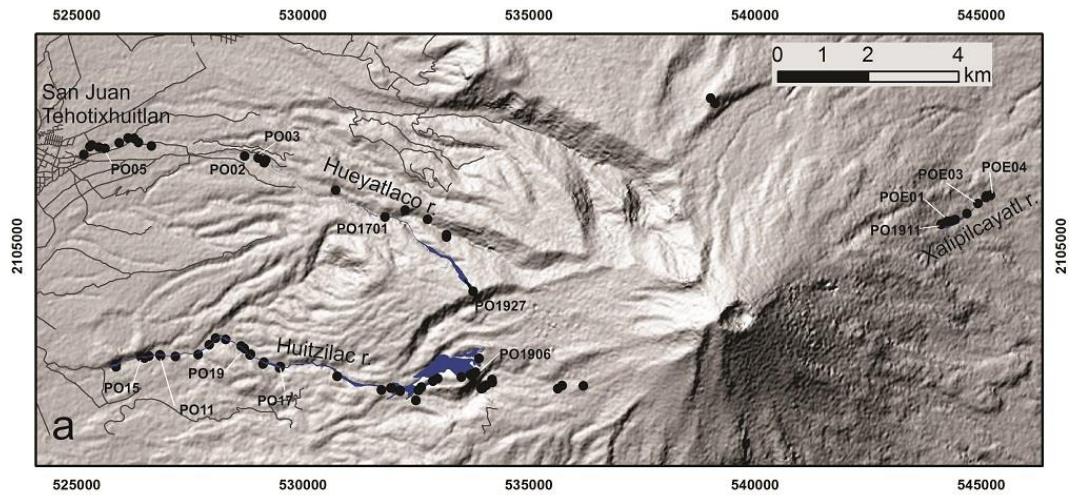


Figure 4: (a) Map of three ravines of the Popocatepetl volcano interested by the debris flows, black dots indicate locations of field surveys (background: 12.5m DEM ©JAXA/METI ALOS PALSAR 2008). (b) View in the downstream direction from the sampling point PO1906 located on the scarp of the Huitzilac landslides n. 1; the profiles of landslides n. 1 and n. 2 are indicated with white lines. (c) Profiles of the three main larger landslide scarps.

4 Results

4.1 Landslide mapping

The earthquake triggered hundreds of shallow landslides (volume > 10³ m³) on the volcano slopes (Figure 3). The largest slope failures are located in the basins of Hueyatlaco (~~one scar~~) and Huitzilac (~~three scars~~) on the West side of the volcanic edifice, and in the basin of Xalipilcayat (~~one scar~~) on the East (Figure 4). These five landslides have been analyzed in detail by using remote sensing imagery, field surveys and laboratory analysis. A second cluster of smaller landslides is visible on the southwestern side of the volcanic cone. These landslides were produced by the collapse of the steep slopes of hummocky hills (dashed circle in Figure 3) that correspond to the debris avalanche deposit of the last major flank failure occurred at 23.5 ka PB (Espinasa-Perena and Martín-Del Pozzo, 2006; Siebe et al., 2017). In the ~~Hueyatlaco three basins~~, where ~~some of~~ the larger landslides occurred, sharp rectilinear extensional fractures and small normal faults ~~opened~~ parallel to the valley slopes (~~Figure 5a~~) were observed (~~Figure 5a~~). These faults and fractures ~~opened during the earthquake and land-sliding event~~, have maximum length of about 1 km, show ~~a recent opening~~/displacements of up to 40-50 cm and are located on the valley flanks (Figure 5b), ~~suggesting a thus they are probably correlated correlation~~ with local gravitational instability triggered by ~~the earthquake seismicity~~.

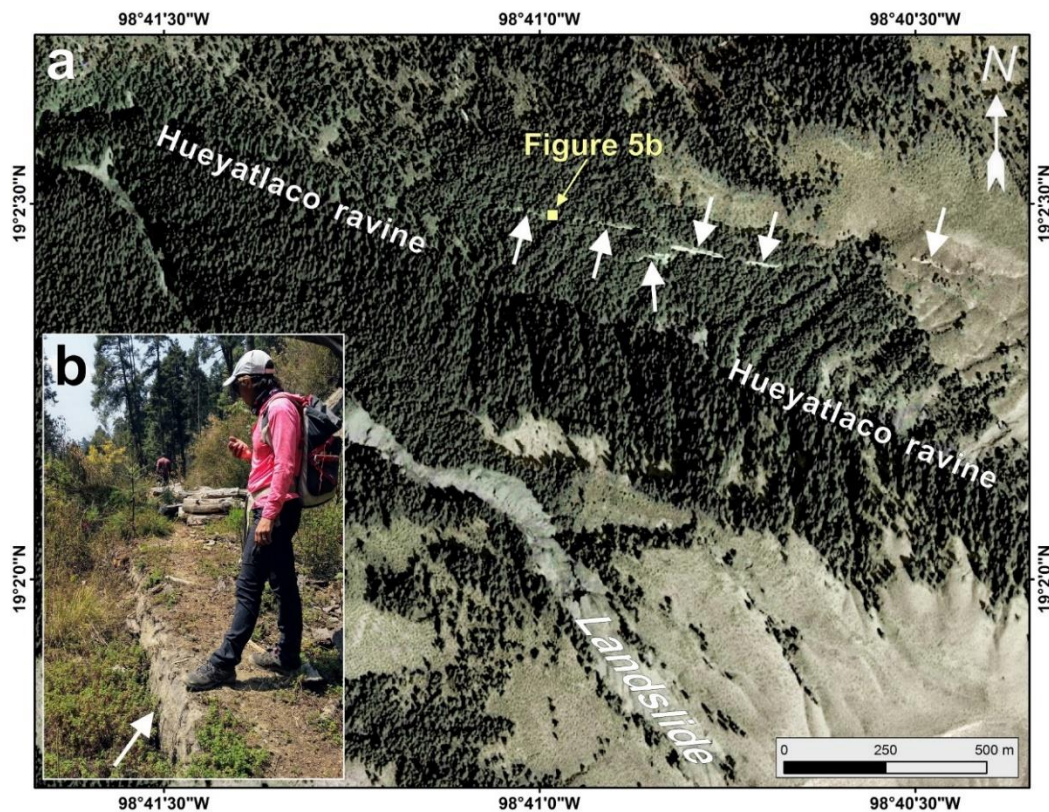


Figure 5: (a) Rectilinear extensional fractures and small normal faults opened parallel to Hueyatlaco ravine (white arrows), background image: Pléiades 1A image acquired on 13 November 2017. (b) Detail of the normal displacement of about 50 cm (white arrow).

Main scarps of the largest slope failures are located at elevations ranging from 3400 to 3800 m a.s.l. and measure 400 m of length and 4 m of depth at Hueyatlaco, 700 m of length and 3 m of depth at Huitzilac, and 200 m of length and 3 m of depth at Xalipilcayatl (Table 1). The scars located on the western slope of the volcano show a very similar stratigraphy, with the intercalation of pumice and ash fall deposits (Figure 6a-c). Pumice fall deposits consist of open-framework, clast-supported units, with gravel-sand sized fragments of pumice, barren of any fine material (silt or clay) into the voids (Table 2). Two main layers of pumice fall deposits were observed at both Hueyatlaco and Huitzilac main landslide scars (layers B and D, section PO1906; layers C and E, section PO1927, Figure 6e). A third pumice fall deposit is outcropping at the base of the sequence. The fallout deposits are intercalated with massive or stratified ash layers, with variable thicknesses up to 4 m. They mainly consist of sand (71-93%), silt (16-1%) and less than 1% of clay (Table 2). A sample from layer C (section PO1906) was dated by using C14, giving a calibrated age 532-639 AD (Figure 6e). Based on this age, the two younger pumice fall deposits are here correlated with the Upper and Lower Classic Plinian Eruptions (UCPES and LCPES) of the late Holocene, which main dispersal axis was towards E and NE (Figure 1b) (Siebe et al., 1996). The thicker deposits of these eruptions crop out on the eastern flank of the volcano, as observed at section PO1911, and correspond to the scar of the Xalipilcayatl landslide (section PO1911; Table 2, Figure 6d). Here, a main unit of pumice fall deposit features a total thickness of 3.5 m, and consists of a massive, clast-supported unit, dominated by gravel pumice fragments, barren of any silt and clay fractions (Table 2). This unit is intercalated towards the base by a 10 cm-thick sandy layer (B, Figure 6d). In all the studied sections, the upper ash unit accumulated from the frequent vulcanian explosions that characterize the modern eruptive activity of the volcano.

Table 1: Main morphometric data of the landslides that occurred in the headwaters of Hueyatlaco, Huitzilac and Xalipilcayatl ravines. The area of the main scars was inferred from field surveys and from the inspection of post-event optical images (see Figure 6). The depth of the scars was measured in the field. The volume of the landslides was calculated assuming a constant depth (with an uncertainty of ± 0.5 m) over the area of detachment.

	Max elevation (m)	Area (m ²)	Depth (m)	Slope	Volume $\times 10^3$ (m ³)
Hueyatlaco	3 860	60 000	4	29	240 \pm 30
Huitzilac	3 700	310 000	3	31-32	930 \pm 155
Xalipilcayatl	3 500	60 000	3	25	180 \pm 30

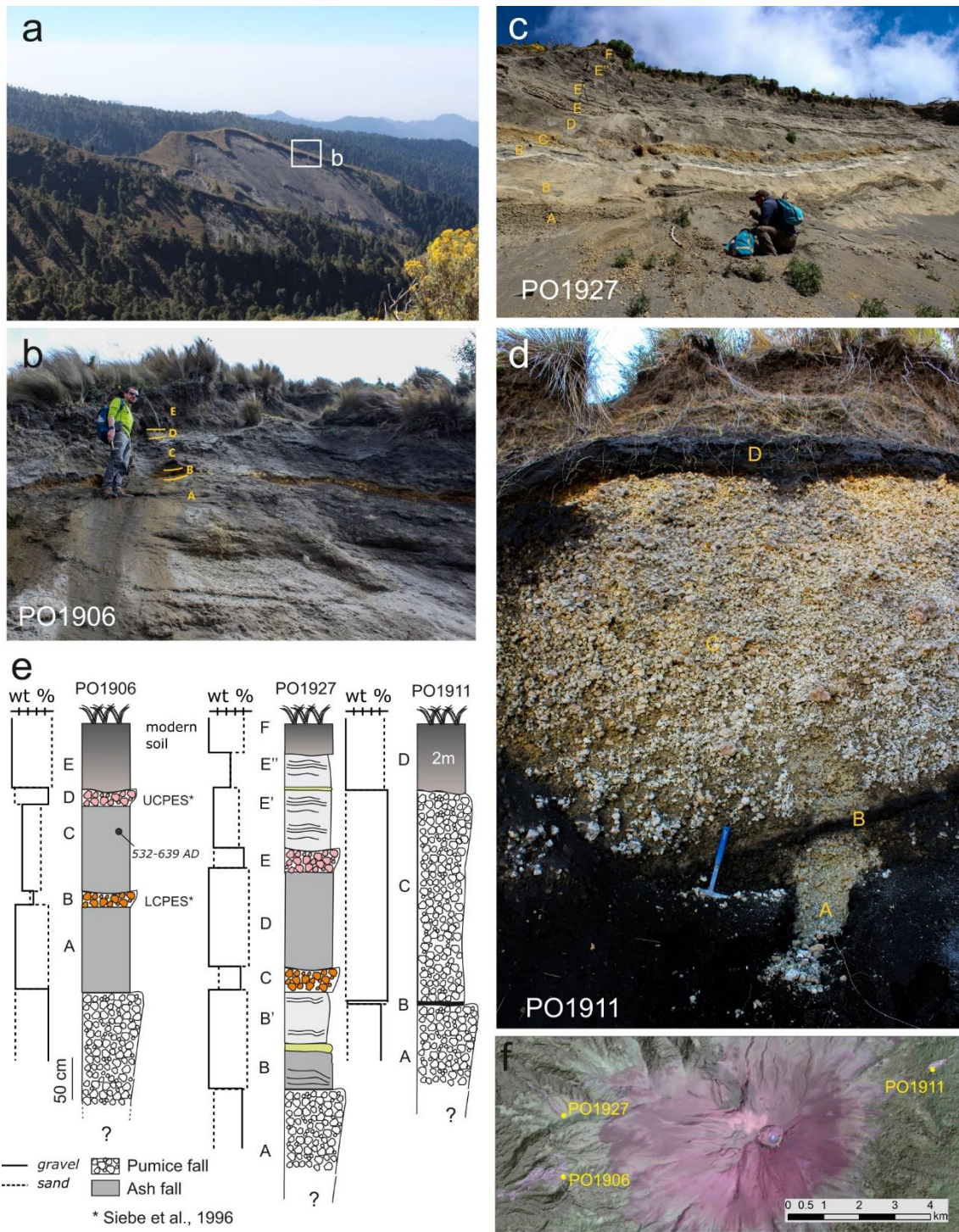


Figure 6: Stratigraphic sections (e) View of the three main landslides scarps: (a, b) Hueyatlaco, (c) Huitzilac, (d) Xalipilcayatl. In (e) the stratigraphic sections of the three scarps are reported, see text for more details. (f) Geographic location of sampling points, background image: Pléiades 1A image acquired on 13 November 2017.

4.2 Characterization of debris flows and associated deposits

The five largest landslides mobilized a total volume of about $1.35 \times 10^6 \text{ m}^3$ of ash and pumice fall deposits (Table 1). The volume of the landslides was calculated assuming a constant depth (with an uncertainty of $\pm 0.5 \text{ m}$) over the area of detachment. The depth of the scars was measured in the field while the area of the main scars was inferred from field surveys and from the inspection of post-event optical images (Figure 7).

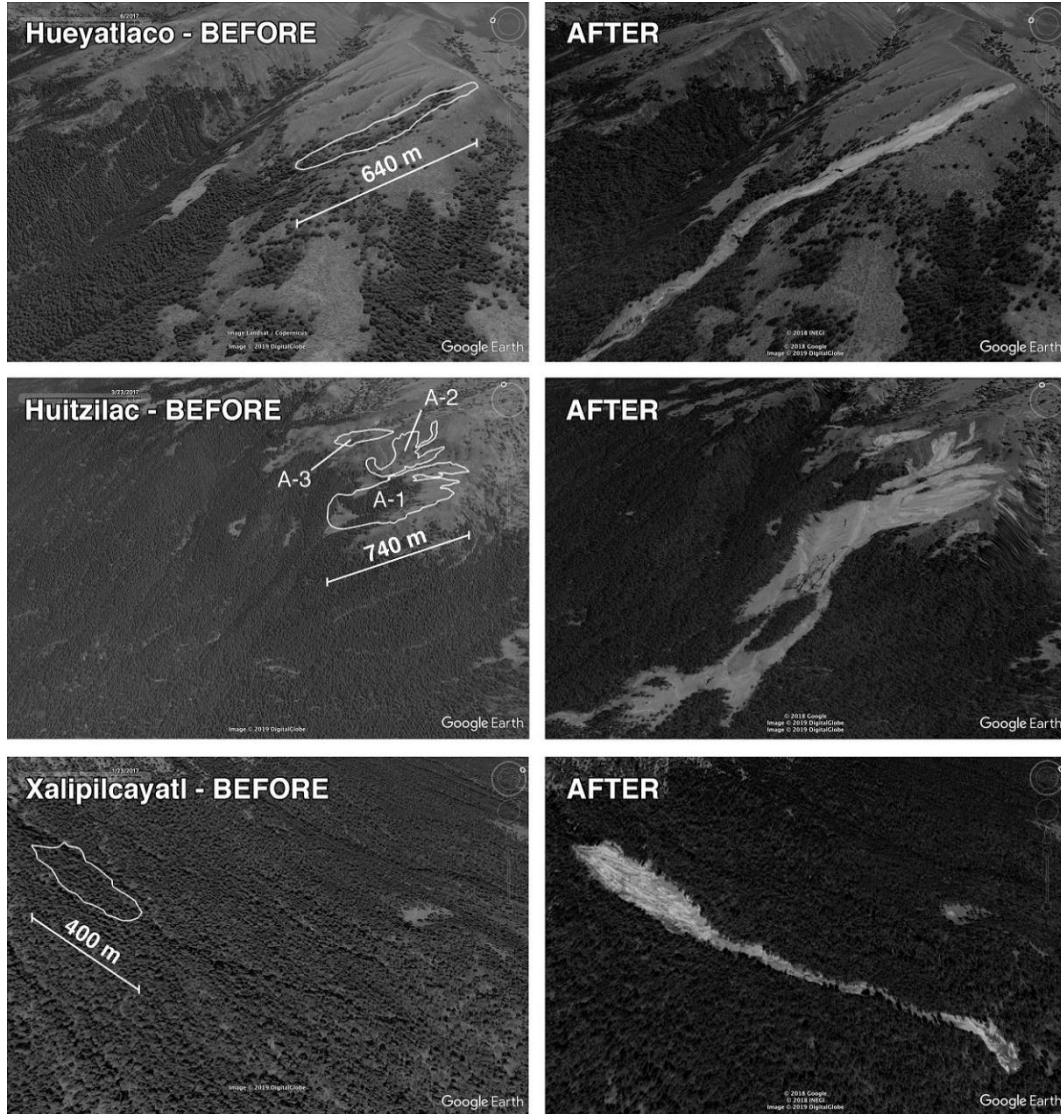


Figure 7: Major landslides that occurred in the headwaters of Hueyatlaco, Huitzilac and Xalipilcayatl ravines. Comparison of 3D views on the detachment areas before and after the landslides. Images from Google Earth (©Google 2018, ©INEGI 2018 and ©DigitalGlobe 2019).

205 The landslides transformed into three long-runout debris flows (Figure 8). At Hueyatlaco ravine, the debris-flow runout extended up to 6.4 km. The deposits appears as a main unit, dark-gray in color, massive and homogeneous whose sand fraction

consists of 70% in proximal reaches (PO1701) to 87% in distal reaches (PO1705), with up to 15% of silt and less than 1% of clay (Figure 6, Table 2). Overbank deposits show sharp edges up to 10-cm thick (PO1702, Figure 8e). The total observed thickness is up to 50 cm (Figure 8d, erosion was only incipient at the time of the observation) but watermarks up to 5 m were observed in proximal reaches (PO1701, Figure 8c). At Huitzilac, the main landslide body (landslide A-1) impacted on the opposite side of the valley, partly overtopping it (Figure 8a). Two other soil slips (landslide A-2 and A-3, Figure 7) contributed forming the subsequent debris flow, which extended up to 7.7 km from the source before diluting into a streamflow. The total observed thickness of the deposit measures up to 3 m, but mud traces on standing trees and on lateral terraces measure up to 10 m on proximal reaches (PO1817, Figure 8b) and up to 1.5 m in distal reaches with horizontal surfaces at benches (PO11, Figure 8f). In distal reaches, where the channel was shallow, the flow inundated large plains (PO1815 and PO1819). The deposit is massive, dark-gray in color, which mainly consists of sand (77-86%) with a relevant gravel proportion (15%) due to pumice fragment enrichment in proximal reaches (Table 2). Clay content is less than 1%. The lower unit consists of ash, mainly sandy, with evidence of dewatering (Figure 8g). Finally, the deposit in the Xalipilcayatl ravine extended up to 1.5 km (Figure 8i) and is clearly composed of two main units. The lower unit is massive, dark-grey in color and mostly consists of sand fraction (88%, POE03-lower, Table 2), up to 1.2 m in thickness, while the upper one is massive, pumice-enriched and represents up to 40% of the total unit (POE04, Figure 8c).

Table 2: Grain size distributions of selected samples collected in the landslide scarps and deposits. Refer to Figure 4 for sample locations.

Landslide scars				
PO1906	Gravel (wt %)	Sand (wt %)	Silt (wt %)	Clay (wt %)
<i>E</i>	3.49	93.14	3.29	0.09
<i>D</i>	87.01	11.94	1.00	0.05
<i>C</i>	26.47	71.90	1.61	0.03
<i>B</i>	54.36	45.12	0.51	0.01
<i>A</i>	13.92	81.00	4.95	0.13
PO1927				
<i>F</i>	0.36	82.18	16.78	0.68
<i>E''</i>	45.75	53.30	0.91	0.04
<i>E'</i>	10.25	76.50	12.73	0.52
<i>E</i>	80.98	16.39	2.45	0.17
<i>D</i>	1.49	87.28	11.12	0.10
<i>C</i>	71.66	27.88	0.45	0.01
<i>B'</i>	0.10	83.89	15.31	0.70
<i>B</i>	0.50	83.77	15.39	0.33
<i>A</i>	80.06	12.40	6.98	0.57
PO1911				
<i>D</i>	0.53	88.55	10.66	0.26
<i>C</i>	94.81	5.19	0.00	0.00

B	4.12	91.84	3.87	0.16
A	89.16	10.37	0.43	0.04
Debris-flow deposits				
<i>Hueyatlaco ravine</i>				
PO1701	17.98	69.20	12.22	0.61
PO02A	19.49	79.05	1.37	0.09
PO02B	5.65	86.42	7.78	0.15
PO02C	4.76	87.52	7.56	0.16
PO05A	6.46	77.81	15.19	0.54
PO05B	2.91	80.49	15.95	0.66
<i>Huitzilac ravine</i>				
PO11	4.25	86.21	9.19	0.34
PO15	0.09	83.54	15.82	0.52
PO17	15.35	77.02	7.41	0.20
PO19	8.49	77.96	13.15	0.38
<i>Xalipilcayatl ravine</i>				
POE04	58.75	36.69	4.25	0.30
POE01	30.77	60.26	8.59	0.36
POE03-upper	62.93	34.45	2.41	0.20
POE03-lower	0.69	88.32	10.63	0.34

225 In the three basins, we estimate a total entrainment of about 200 000 m³ along both hillslopes and channel network (Table 3). Large wood (LW) elements entrained by the initial landslides and the subsequent debris flows contributed to the final bulk deposits of about 1.63 × 10⁶ m³. The amount of LW recruited in the Huitzilac basin results in 60 000 m³ (± 3 000 m³), far more than the sum of Hueyatlaco (10 000 ± 500 m³) and Xalipilcayatl (7 000 ± 350 m³) basins. The volume of LWs was calculated considering a mean tree height of 25 m (measured in the field, with an uncertainty of ±5 m), a mean trunk diameter of 0.4 m

230 (observed in the field, with an uncertainty of ±0.1 m) and a mean distance of two trees of 10 m (estimated by using the post-event optical images, see Figure 7). The recruited LW stemmed from the combination of hillslope and channel processes originated from the earthquake-induced landslides. In general, these landslides were the dominant recruitment processes in headwaters. In contrast, LW recruitment from lateral bank erosion became significant in the intermediate reaches of the channels. The slope area collapsed into the Xalipilcayatl basin contained most of the LWs afterwards transported by the flow

235 (86%). In the Huitzilac basin the LW recruitment mainly occurred on the slopes located right below the collapses (62%), while in the Hueyatlaco basin on the channel banks (75%). Most of the transported LWs remained trapped by natural obstacles in the main channel (i.e. standing vegetation) and clogged in the flat reaches of the channel (Figure 8d). In the Xalipilcayatl ravine, most of LWs were transported for the whole runout distance into the main landslide deposit (Figure 8i).



240 **Figure 8:** Debris-flow deposits in the upper (a-c), intermediate (d-f) and lower reaches (g-i) of Huitzilac, Hueyatlaco and Xalipilcayatl
 basins: (a) scarp of landslide A-1 at Huitzilac, (b) main channel of Huitzilac ravine (PO1817), (c) main channel of Hueyatlaco ravine
 (PO1701), (d) large wood deposits at Hueyatlaco (PO03), (e) overbank deposits at Hueyatlaco (PO1702), (f) mud trace on lateral terraces at
 Huitzilac, **HWM = Height of Water Mark** (PO11), (g) evidence of dewatering at Huitzilac (PO1819), (h) detail of the lower deposit at
 Xalipilcayatl (POE04), (i) main channel right upstream the deposition area at Xalipilcayatl.

245

Table 3: Main morphometric data of the debris flows that were observed in the Hueyatlaco, Huitzilac and Xalipilcayatl basins. The entrained volume was calculated assuming 0.5 m of erosion over the area located downstream from the main scars where the vegetation was destroyed. The volume of large wood (LW) fragments was calculated considering a mean tree height of 25 m (with an uncertainty of ± 5 m), a mean trunk diameter of 0.4 m (with an uncertainty of ± 0.1 m) and a mean distance of two trees of 10 m.

	Runout (km)	Drop height (m)	Entrainment $\times 10^3$ (m ³)	LW volume $\times 10^3$ (m ³)
Hueyatlaco	6.4	1 160	50	10 ± 0.5
Huitzilac	7.7	1 200	120	60 ± 3
Xalipilcayatl	1.5	350	35	7 ± 0.35

250 4.3 Timing of the events

Results of Sentinel-1 SAR image processing clearly indicate that both landslides and debris flows had already occurred between 17 and 23 September 2017. A binary image was produced where pixels values are linked to spatial change that occurred in this span of time (Figure 9a). Their distribution corresponds with the deposits of the larger debris flows that occurred in Huitzilac and Hueyatlaco basins, as it is easily observable in a later optical Sentinel-2 image (COPERNICUS

255 program) acquired on 18 October 2017 (Figure 9b).

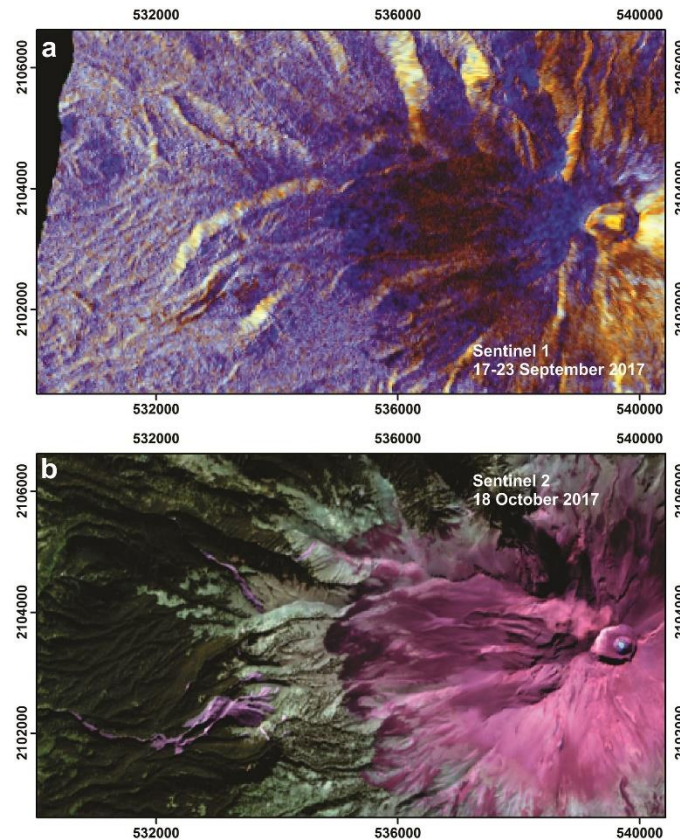


Figure 9: (a) RGB (R, post-earthquake, G, pre-earthquake, B, ratio between post and pre event) representation of the 17 and 23 September Sentinel-1 (©Copernicus data) change in amplitude analysis; (b) RGB composition of post-event Sentinel-2 image (©Copernicus data).

A total of 200 mm of accumulated rainfall were recorded during the 30 days preceding the earthquake, with the accumulation of 19.7 mm two days before the earthquake (Figure 10). Thus, we expect that the slope material was wet at the time of the earthquake. Based on the remote sensing analysis and considering that between 19 and 23 September only a few mm of rainfall accumulated (Figure 10), it is thus highly probable that both slope failures and debris-flow emplacement were co-seismic. Witnesses from the town of Atlautla, which is located at the outlet of Huitzilac ravine, also confirmed this information. During the following weeks, rainfalls remobilized fine material from the landslide deposits reaching the town of San Juan Tehuixtitlán (Figure 4a). On 4 October 2017 the population of San Juan Tehuixtitlán noticed the transformation of the shallow water-flow of Hueyatlaco ravine into a high-concentrated, slow-moving debris-flow. It is the first time that this local community located on the western volcano slope observed such a phenomenon. Rainfall measurement at Altzomoni raingauge station (Figure 1b) shows an accumulation of 35.7 mm of rainfall over 12 hours since 10 hrs (24 hr UTC time) of 4 October, with a peak between 20 and 21 hr (Figure 10). The rainfall event of 4 October only remobilized fine material from the landslide deposits reaching the town of San Juan Tehuixtitlán; the debris flows along the Huitzilac and Xalipilcayatl were never reported since they never extended out to any populated area in 2017. During the 2018 rainy season, in Huitzilac ravine the fine sediment remobilized from the debris flow deposit and reached the bridge of the road connecting Amecameca to Atlautla.

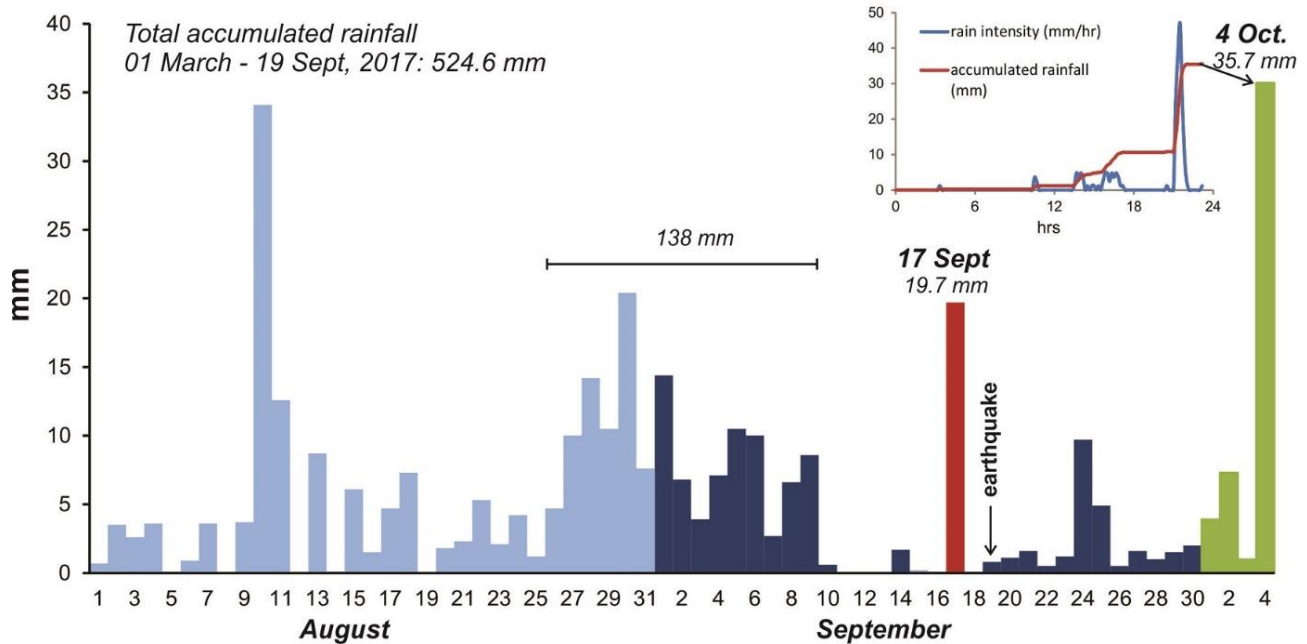
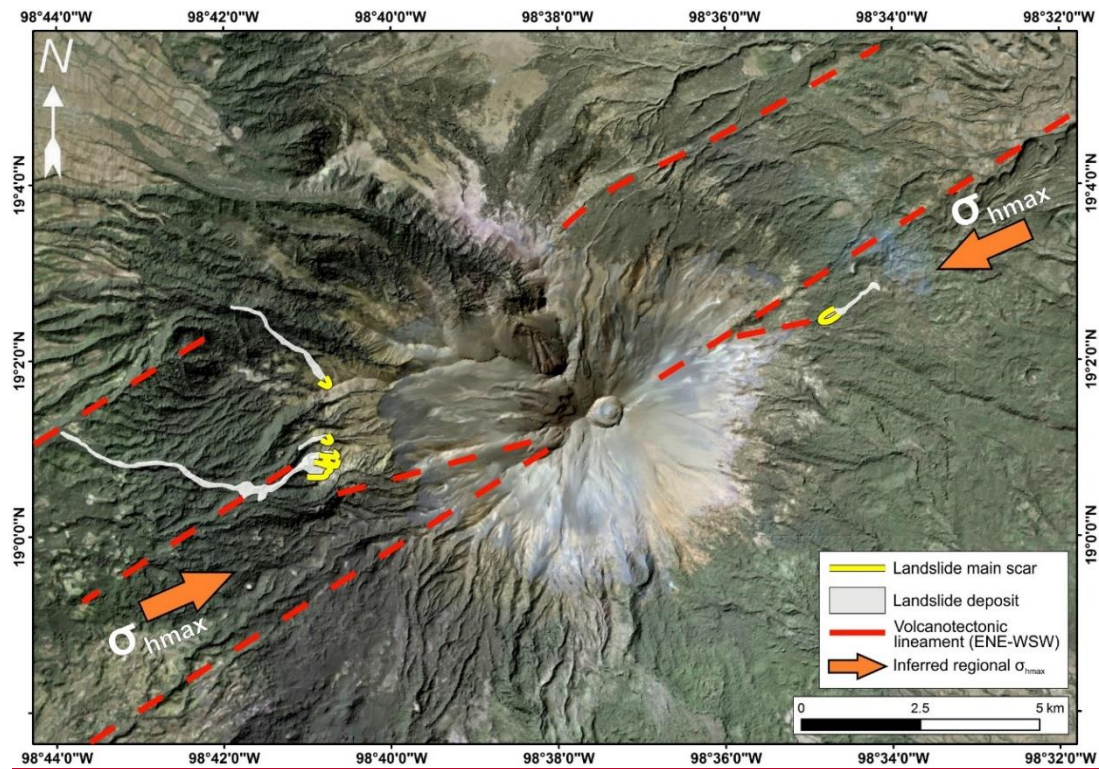


Figure 10: Rainfall measurements at rain gauge ALTZ from 1 August to 4 October 2017.

5.1 Predisposing factors to slope instabilities

Popocatepetl area is tectonically characterized by a Quaternary roughly NE-SW/ENE–WSW trending maximum horizontal stress regime, responsible for arc-parallel E-W-striking transtensive faults and NE-SW/ENE–WSW arc-oblique normal faults (Arámbula-Mendoza et al., 2010; García-Palomo et al., 2018; Norini et al., 2006, 2019). This stress regime generated ENE–
 280 WSW extensional fracturing and faulting of the volcanic edifice (Figure 11), controlling the orientation and propagation by magmatic overpressure of dikes within the volcanic cone and recent eruptive fissures on its flanks (Arámbula-Mendoza et al., 2010; De Cserna et al., 1988).

On 19 September 2017, Popocatepetl volcano underwent co-seismic slope failures (Figure 2). The size of these slope failures greatly changes with the location with respect to the cone's summit, although even if (i) the epicenter of the earthquake is far
 285 from the volcano, with seismic shaking expected to be of similar intensity all over the symmetric volcanic cone, and (ii) soil and recent pyroclastic cover is quite homogeneous on the edifice flanks. Small landslides occurred all over the volcano flanks, while the few larger landslides described in our work are limited to the eastern and western sides of the volcanic cone (Figure 3). Thus, seismic shaking originated by the far earthquake triggered large (volume > 10^5 m³) landslides only in specific sectors of the volcano flanks.



290

Figure 11: Simplified tectonic setting of the Popocatepetl area and location of the main ~~landslides~~ earthquake-induced landslides that occurred on 2017. Background image: ©DigitalGlobe/ESRI 2019.

The symmetric location of the larger slope failures defines a sharp ENE-WSW unstable sector crossing the volcano summit and parallel to many deep rectilinear valleys carved in the volcanic cone (Figure 11). In this ENE-WSW elongated sector of the volcano, some faults and extensional fractures have been generated by the 2017 earthquake in the same basins where the larger landslides occurred (Figure 5). This configuration may suggest strongly localized site effects and/or a structural control on the location of the slope instability. Indeed, the unstable sector is roughly parallel to the ENE-WSW maximum horizontal stress, where local volcanotectonic structural features are recognized on the volcano (Arámbula-Mendoza et al., 2010; De Cserna et al., 1988). The remobilization of larger quantities of material in this sector with respect to other areas of the volcano flanks may be correlated to the presence of ENE-WSW-striking faults and fractures that progressively weakened the volcanic edifice. Some of these volcanotectonic structures may also have undergone transient reactivation by seismic shaking, increasing local slope deformation by opening of fractures that promoted the largest slope failures triggered by the earthquake.

5.2 Initiation of co-seismic landslides

Slopes collapse when the shear stress across a potential failure plane exceeds the substrate strength. Earthquakes reduce the slope stability and can cause landslides through the perturbation of the normal and shear stresses in the slope. In case of soft, saturated soils, the coalescence of cracks during earthquakes may result in liquefaction due to the increase of substrate permeability. At Popocatepetl volcano, a combination of these two mechanisms produced the soil slips observed in the headwaters of Hueyatenco, Huitzilac, and Xalipilcayatl basins. Shapiro et al. (2000) already noticed that a large earthquake occurring in the vicinity of the volcano may result in flank instability because of the seismic waves traversing the poorly consolidated material composing the volcanic edifice.

Unexpected large peak accelerations have been recorded along crests of mountain ridges during several earthquakes (Bouchon et al., 1996; Davis and West, 1973; Geli et al., 1988; Meunier et al., 2008). Topographic amplification of ground vibrations is due to the reflection/diffraction of seismic waves (Bouchon et al., 1996). Seismic waves are progressively focused upwards and the constructive interference of their reflections and the associated diffractions increases towards the ridge crest, giving rise to enhanced ground accelerations on topographic highs (Meunier et al., 2008). Geli et al., (1988) show that the topographic complexity (presence of neighboring ridges) may be responsible for large crest/base amplifications resulting in complex amplification-deamplification patterns and significant differential motions along the slopes. The amplification at the crest of a mountain can be as large or larger than the amplification normally caused by the presence of near-surface unconsolidated layers (Davis and West, 1973).

It is well-known that shallower earthquakes may cause large landslides (e.g., Marc et al., 2019), but the Puebla-Morelos earthquake was moderately deep (i.e., 57 km). The PGA produced by the 2017 earthquake at station PPIG (158.16 cm/s^2) was about three times higher than the PGA observed at CU (57.1 cm/s^2). Indeed, the distance epicenter-PPIG (68 km) is about half than the distance epicenter-CU (111 km) and this partially explains the difference in PGA observed at the two stations. However, during the earthquake the headwaters of Hueyatenco, Huitzilac, and Xalipilcayatl ravines could have experienced even higher values of PGA due to the effect of topographic amplification of seismic waves. The complex topography of

Popocatepetl volcano, characterized by neighboring ridges and valleys, probably produced local amplification values that makes it difficult to explain why larger soil slips did not occur in other similar locations in terms of elevation, slope and stratigraphy. However, the deposits located along the ENE-WSW unstable sector of the volcano (see previous paragraph), at an elevation ranging from 3400 to 3800 m and characterized by a slope $> 20^\circ$, appear as the most likely to suffer collapse in case of an earthquake. This sector of Popocatepetl volcano consists of a mantle of loose volcanoclastic material with the intercalation of silty-sandy ash layers and gravel-sand pumice fall deposits (up to 5-m thick, see Figure 6), covered by a modern soil with thick alpine grassland. At higher altitude, the steeper slopes are unvegetated, and consist of unconsolidated pyroclastic granular material where superficial granular flows can be easily observed. The largest landslides occurred in the limit of the vegetation line, where pine trees became scattered but grassland is still abundant (Figure 2). The intercalation of layer with different grain size and the soil coverage are probably promoting water accumulation. Indeed, one mechanism that possibly can explain the collapse of this material is the liquefaction through the disruption of internal, suspended aquifers. A similar observation was recently made at Nevado del Huila Volcano, Colombia, during 2007 when lahars originated after large fractures formed across the summit area of the volcano in consequence of a strong hydromagmatic explosion that drained small, perched aquifers (Johnson et al., 2018). On the unvegetated portion of the cone, mass remobilization processes such as raveling and superficial granular flows likely occurred but without leaving any scarp, because of the lack of a compacted soil.

5.3 Transformation into long runout debris flows and implications for hazard assessment

Once generated, the earthquake-induced soil slips transformed into debris flows. The two major debris flows that occurred in Hueyatenco and Huitzilac basins covered a runout distance of 6.4 and 7.7 km, respectively. In Figure 12 we show the conceptual model of this transformation at Popocatepetl volcano: ~~the~~ propagation of an earthquake-induced crack in the slope (1) produces a shallow landslide composed of a mix of ash and pumice (2). The ~~landslide collapsed material disgregates,~~ impacts on the opposite side of the valley and rapidly ~~the landslide~~ evolves into debris flows, due to the high water content of the collapsed material. The subsequent debris flow is highly viscous due to the high sand and silt fraction of the mixture and contains abundant LWs entrained along the channel network (3), especially along the Huitzilac and Xalipilcayatl channels which had entire mature ~~forests-trees~~ incorporated, thus leaving abundant log-strewn debris. Even if no direct observations are available to assume if the collapsed slopes were partially or completely saturated, it is clear that debris flows contained a large amount of water as observed from dewatering features of the deposits and high water marks along the channels (Figure 8g). Since August 21, 138 mm of rainfall accumulated continuously for two weeks, and 19.7 mm just two days before the earthquake (Figure 10). This large amount of rainfall was then stored in the open-framework pumice fall deposits intercalated by m-thick sandy layers and in the root fabric of the trees in the dense forest cover. ~~Volcanoes store or drain water in and through aquifers that can develop and empty, as impermeable barriers develop or as they are breached by deformation, respectively~~ (Delcamp et al., 2016). ~~Even if~~ not completely saturated, ground vibrations induced positive pore pressure and triggered liquefaction and slopes failure (Kameda et al., 2019; Wang et al., 2019). It is important to note that on August 10 a rainfall of 35 mm, similar to the October 4 event that triggered the sediment-laden flow observed at San Juan Tehuixtitlán

village, did not induce any channel response, indicating the stability of the slopes of this sector of the volcano prior to the earthquake. In fact, except for the 2010 lahar that occurred in the Nexplayantla ravine after 100 mm of accumulated rainfall (Zaragoza-Campillo et al., 2020), lahars are related to major eruptions, reason for which the actual hazard map of the Popocatépetl volcano includes only rainfall-triggered lahar during or after eruptions (Martin Del Pozzo et al., 2017). Detailed field investigations of the role of aquifer on volcanic landslides are very scarce to the date (Delcamp et al., 2016). Knowledge of the distribution of perched aquifers and water content of volcanic deposits can provide precious insights on a complex mass wasting chain like the one that experienced Popocatépetl volcano in 2017.

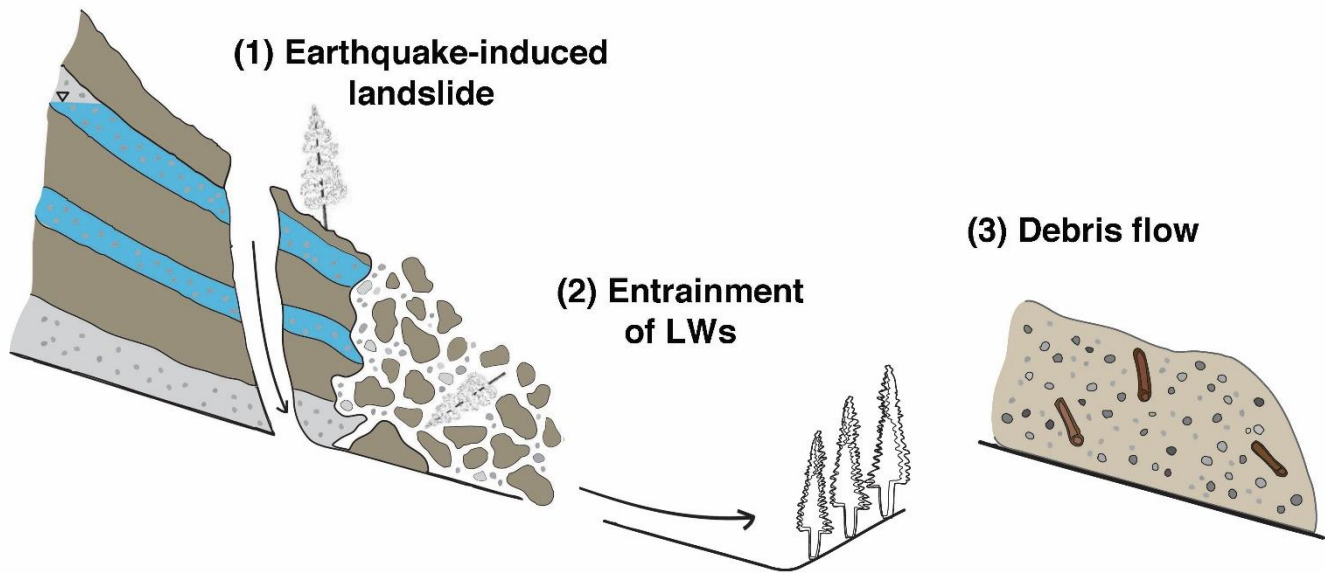


Figure 12: Conceptual model of transformation of earthquake-induced soil slips into debris flows at Popocatépetl volcano: (1) the earthquake produces the collapse of the saturated slope composed of a mix of ash and pumice; (2) the landslide impacts on the opposite side of the valley entraining a large amount of Large Woods (LWs) and (3) evolves into a debris flow due to the high water content of the material. The simplified stratigraphy in (1) reflects the one observed at the scar of Huitzilac landslide (see Figure 6c).

6 Conclusions

Landslides represent one of the most dangerous phenomena that may occur on active volcanoes. The combination of earthquake and volcanic activity can result in large mass movements and subsequent floods that can dramatically increase the sediment load along the drainage network. In this work, we present the earthquake-induced landslides that occurred on 17 September 2017. A total volume of about 10^6 cubic meter of volcanoclastic deposits collapsed and transformed in two large debris flows on the western slope of the volcano and one on its eastern side. This is the first time that such large wood-strewn debris flows were directly observed at this volcano. These observations imply the need to revise the hazards assessment for Popocatépetl volcano, where multi-hazard risk scenarios (i.e., combination of a large earthquake and landslides transforming into long-runout debris flows) should be taken into account. Seeing such deposits in the geologic record could also cause

380 confusion with identifying them with primary lahars. ~~Thus studies such as this one, are an opportunity to point out what such earthquake lahars look like in the Mexican highlands.~~ The mass-wasting cascade observed and here described may occur in other areas, especially continental volcanic arcs [and mountain chains in seismic regions](#), worldwide.

Acknowledgements. This research is supported by the CONACYT-PN 360 project and the EARFLOW project, funded by the MAECI - Ministero degli Affari Esteri e della Cooperazione Internazionale and the AMEXCID - Agencia Mexicana de Cooperación Internacional para el Desarrollo. Seismic data were provided by the Servicio Sismológico Nacional (SSN - UNAM, México). Rainfall data were kindly provided by Adolfo Magalli. This paper is supported by the Open Access Publishing Fund of the Free University of Bozen-Bolzano. We thank Berlaine Ortega-Flores, Lizeth Cortez and Lizeth Caballero for their support in the field and in the laboratory.

Data availability. Samples collected on landslide scars and deposits are stored at CGEO-UNAM. Rainfall data at Altzomoni rain gauge station (ALTZ, RUOA-UNAM) are available at <https://www.ruoa.unam.mx/index.php?page=estaciones>. Sentinel-1 and Sentinel-2 images (©Copernicus data) acquired on 17 and 23 September 2017 are available at <https://scihub.copernicus.eu/>. The 50-cm resolution Pléiades (AIRBUS) optical image acquired on 13 November 2017 was bought by the authors, a preview of this image is available at https://www.intelligence-airbusds.com/satellite-image/?id=DS_PHR1A_201711131716409_FR1_PX_W099N18_0516_07848.

395 *Author contributions.* VC and LC conceived the idea and planned the work. VC, LC, GN, DF and EP performed the field work and collected samples of landslide scars and deposits. VC, LC and GN wrote most part of the manuscript. VM analyzed seismic data of the PPIG station (SSN-UNAM). ND processed Sentinel-1 and Sentinel-2 images. EP analyzed the post-event Pléiades image and drew the landslide map. All the authors discussed the results and commented on the manuscript.

Competing interests. The authors declare that they have no conflict of interest.

400 **References**

- Almeida, L., Cleef, A. M., Herrera, A., Velazquez, A. and Luna, I.: El zacatonal alpino del Volcán Popocatepetl, México, y su posición en las montañas tropicales de América, *Phytocoenologia*, 22(3), 391–436, doi:10.1127/phyto/22/1994/391, 1994.
- Arámbula-Mendoza, R., Valdés-González, C. and Martínez-Bringas, A.: Temporal and spatial variation of the stress state of Popocatepetl Volcano, Mexico, *J. Volcanol. Geotherm. Res.*, 196(3–4), 156–168, doi:10.1016/j.jvolgeores.2010.07.007, 2010.
- 405 Bouchon, M., Schultz, C. A. and Toksoz, M. N.: Effect of three-dimensional topography on seismic motion, *J. Geophys. Res.*, 101(B3), 5835–5846, 1996.
- Camacho, H.: Efectos del temblor sobre el terrano: Chapter V, Tercera Parte, in *Memoria Relativa al Terremoto Mexicano del 3 de Enero de 1920*, pp. 89–94., 1920.
- Capra, L., Poblete, M. A. and Alvarado, R.: The 1997 and 2001 lahars of Popocatepetl volcano (Central Mexico): Textural and sedimentological constraints on their origin and hazards, *J. Volcanol. Geotherm. Res.*, 131(3–4), 351–369, doi:10.1016/S0377-0273(03)00413-X, 2004.
- 410 Capra, L., Bernal, J. P., Carrasco-Núñez, G. and Roverato, M.: Climatic fluctuations as a significant contributing factor for volcanic collapses. Evidence from Mexico during the Late Pleistocene, *Glob. Planet. Change*, 100, 194–203,

- doi:10.1016/j.gloplacha.2012.10.017, 2013.
- 415 Capra, L., Coviello, V., Borselli, L., Márquez-Ramírez, V.-H. and Arámbula-Mendoza, R.: Hydrological control of large hurricane-induced lahars: evidences from rainfall, seismic and video monitoring, *Nat. Hazards Earth Syst. Sci.*, 18(October), 781–794, doi:10.5194/nhess-2017-354, 2018.
- Castillo, M., Muñoz-Salinas, E. and Arce, J. L.: Evaluación del sistema erosivo fluvial en el volcán Popocatepetl (México) mediante análisis morfométricos, *Bol. la Soc. Geol. Mex.*, 67(2), 167–183, 2015.
- 420 De Cserna, Z., De la Fuente-Duch, M., Palacio-Neto, M., Triay, L., Mitre-Salazar, L. M. and Mota-Palomino, R.: Estructura geológica, gravimétrica y relaciones neotectónicas regionales de la Cuenca de México, *Bol. Inst. Geol. UNAM.*, 104, 71, 1988.
- Dadson, S. J., Hovius, N., Chen, H., Dade, W. B., Lin, J. C., Hsu, M. L., Lin, C. W., Horng, M. J., Chen, T. C., Milliman, J. and Stark, C. P.: Earthquake-triggered increase in sediment delivery from an active mountain belt, *Geology*, 32(8), 733–736, doi:10.1130/G20639.1, 2004.
- 425 Davis, L. L. and West, L. R.: Observed effects of topography on ground motion, *Bull. Seismol. Soc. Am.*, 63(1), 283–298, 1973.
- Delcamp, A., Roberti, G. and van Wyk de Vries, B.: Water in volcanoes: evolution, storage and rapid release during landslides, *Bull. Volcanol.*, 78(12), doi:10.1007/s00445-016-1082-8, 2016.
- Espinasa-Perena, R. and Martín-Del Pozzo, A. L.: Morphostratigraphic evolution of popocatepetl volcano, México, *Spec. Pap. Geol. Soc. Am.*, 402(05), 115–137, doi:10.1130/2006.2402(05), 2006.
- 430 Flores, T.: Efectos geologicos: Chapter IV, Primera Parte, in *Memoria del terremoto Mexicano del 3 de enero de 1920*, pp. 27–29., 1922.
- García-Palomo, A., Macías, J. L., Jiménez, A., Tolson, G., Mena, M., Sánchez-Núñez, J. M., Arce, J. L., Layer, P. W., Santoyo, M. Á. and Lermo-Samaniego, J.: NW-SE Pliocene-Quaternary extension in the Apan-Acozulco region, eastern Trans-Mexican
- 435 Volcanic Belt, *J. Volcanol. Geotherm. Res.*, 349, 240–255, doi:10.1016/j.jvolgeores.2017.11.005, 2018.
- Geli, L., Bard, P. and Jullien, B.: THE EFFECT OF TOPOGRAPHY ON EARTHQUAKE GROUND MOTION: A REVIEW AND NEW RESULTS, *Bull. Seismol. Soc. Am.*, 78(1), 42–63, 1988.
- Johnson, P. J., Valentine, G. A., Stauffer, P. H., Lowry, C. S., Sonder, I., Pulgarín, B. A., Santacoloma, C. C. and Agudelo, A.: Groundwater drainage from fissures as a source for lahars, *Bull. Volcanol.*, 80(4), doi:10.1007/s00445-018-1214-4, 2018.
- 440 Julio-Miranda, P., Delgado-Granados, H., Huggel, C. and Käab, A.: Impact of the eruptive activity on glacier evolution at Popocatepetl Volcano (México) during 1994-2004, *J. Volcanol. Geotherm. Res.*, 170(1–2), 86–98, doi:10.1016/j.jvolgeores.2007.09.011, 2008.
- Kameda, J., Kamiya, H., Masumoto, H., Morisaki, T., Hiratsuka, T. and Inaoi, C.: Fluidized landslides triggered by the liquefaction of subsurface volcanic deposits during the 2018 Ibuli-Tobu earthquake, *Hokkaido, Sci. Rep.*, 9(1), 1–6,
- 445 doi:10.1038/s41598-019-48820-y, 2019.
- Keefer, D. K.: Landslides caused by earthquakes, *GSA Bull.*, 95(2), 406–421, doi:10.1016/0148-9062(85)92394-0, 1984.
- Keefer, D. K., Wartman, J., Navarro Ochoa, C., Rodriguez-Marek, A. and Wicczorek, G. F.: Landslides caused by the M 7.6

- Tecomán, Mexico earthquake of January 21, 2003, *Eng. Geol.*, 86(2–3), 183–197, doi:10.1016/j.enggeo.2006.02.017, 2006.
- Major, J. J., Bertin, D., Pierson, T. C., Amigo, A., Iroumé, A., Ulloa, H. and Castro, J.: Extraordinary sediment delivery and rapid geomorphic response following the 2008–2009 eruption of Chaitén Volcano, Chile, *Water Resour. Res.*, 52, 5075–5094, doi:10.1002/2015WR018250. Received, 2016.
- Manville, V., Németh, K. and Kano, K.: Source to sink: A review of three decades of progress in the understanding of volcanoclastic processes, deposits, and hazards, *Sediment. Geol.*, 220(3–4), 136–161, doi:10.1016/j.sedgeo.2009.04.022, 2009.
- Marc, O., Behling, R., Andermann, C., Turowski, J. M., Illien, L., Roessner, S. and Hovius, N.: Long-term erosion of the Nepal Himalayas by bedrock landsliding: The role of monsoons, earthquakes and giant landslides, *Earth Surf. Dyn.*, 7(1), 107–128, doi:10.5194/esurf-7-107-2019, 2019.
- Martin Del Pozzo, A. L., Alatorre Ibarquiengoitia, M., Arana Salinas, L., Bonasia, R., Capra Pedol, L., Cassata, W., Córdoba, G., Cortés Ramos, J., Delgado Granados, H., Ferrés López, M. D., R., F. Á., García Reynoso, J. A., Gisbert, G., Guerrero López, D. A., Jaimes Viera, M. C., Macías Vázquez, J. L., Nieto Obregón, J., Nieto Torres, A., Paredes Ruiz, P. A., Portocarrero Martínez, J., Renne, P., Rodríguez Espinosa, D. M., Salinas Sánchez, S., Siebe Grabach, C. and Tellez Ugalde, E.: Estudios geológicos y actualización del mapa de peligros del volcán Popocatepetl, *Monografías Instituto de Geofísica, UNAM.*, 2017.
- Mcguire, W. J.: Volcano instability: A review of contemporary themes, *Geol. Soc. Spec. Publ.*, 110(110), 1–23, doi:10.1144/GSL.SP.1996.110.01.01, 1996.
- Melgar, D., Pérez-Campos, X., Ramirez-Guzman, L., Spica, Z., Espíndola, V. H., Hammond, W. C. and Cabral-Cano, E.: Bend Faulting at the Edge of a Flat Slab: The 2017 Mw7.1 Puebla-Morelos, Mexico Earthquake, *Geophys. Res. Lett.*, 45(6), 2633–2641, doi:10.1002/2017GL076895, 2018.
- Meunier, P., Hovius, N. and Haines, J. A.: Topographic site effects and the location of earthquake induced landslides, *Earth Planet. Sci. Lett.*, 275(3–4), 221–232, doi:10.1016/j.epsl.2008.07.020, 2008.
- Mondini, A. C.: Measures of spatial autocorrelation changes in multitemporal SAR images for event landslides detection, *Remote Sens.*, 9(6), doi:10.3390/rs9060554, 2017.
- Norini, G., GropPELLI, G., Lagmay, A. M. F. and Capra, L.: Recent left-oblique slip faulting in the central eastern Trans-Mexican Volcanic Belt: Seismic hazard and geodynamic implications, *Tectonics*, 25, 1–21, doi:10.1029/2005TC001877, 2006.
- Norini, G., Capra, L., GropPELLI, G. and Lagmay, A. M. F.: Quaternary sector collapses of Nevado de Toluca volcano (Mexico) governed by regional tectonics and volcanic evolution, *Geosphere*, 4(5), 854–871, doi:10.1130/GES00165.1, 2008.
- Norini, G., Carrasco-Núñez, G., Corbo-Camargo, F., Lermo, J., Rojas, J. H., Castro, C., Bonini, M., Montanari, D., Corti, G., Moratti, G., Piccardi, L., Chavez, G., Zuluaga, M. C., Ramirez, M. and Cedillo, F.: The structural architecture of the Los Hornos volcanic complex and geothermal field, *J. Volcanol. Geotherm. Res.*, 381, 312–329, doi:10.1016/j.jvolgeores.2019.06.010, 2019.
- Pasquaré, G., Vezzoli, L. and Zanchi, A.: Morphological and structural model of Mexican Volcanic Belt, *Geofísica Int.*, 26.2,

- 159–175, 1987.
- Pearce, A. J. and Watson, A. J.: Effects of earthquake-induced landslides on sediment budget and transport over 50-yr period, *Geology*, 14, 52–55, 1986.
- 485 Roberti, G., Friele, P., van Wyk de Vries, B., Ward, B., Clague, J. J., Perotti, L. and Giardino, M.: Rheological evolution of the Mount Meager 2010 debris avalanche, southwestern British Columbia, *Geosphere*, 13(2), 1–22, doi:10.1130/GES01389.1, 2017.
- Roverato, M., Cronin, S., Procter, J. and Capra, L.: Textural features as indicators of debris avalanche transport and emplacement, Taranaki volcano, *Bull. Geol. Soc. Am.*, 127(1–2), 3–18, doi:10.1130/B30946.1, 2015.
- 490 Sassa, K.: Landslide disasters triggered by the 2004 Mid-Niigata Prefecture earthquake in Japan, *Landslides*, 2(2), 135–142, doi:10.1007/s10346-005-0054-4, 2005.
- Scott, K. M., Macias, J. L., Naranj, J. A., Rodriguez, S. and McGeehin, J. P.: Catastrophic debris flows transformed from landslides in volcanic terrains: mobility, hazard assessment and mitigation strategies, USGS Professional Paper 1630., 2001.
- Shapiro, N. M., Singh, S. K., Iglesias-Mendoza, A., Cruz-Atienza, V. M. and Pacheco, J. F.: Evidence of low Q below
495 Popocatepetl volcano, and its implication to seismic hazard in Mexico City, *Geophys. Res. Lett.*, 27(17), 2753–2756, doi:10.1029/1999GL011232, 2000.
- Siebe, C. and Macías, J. L.: Volcanic hazards in the Mexico City metropolitan area from eruptions at Popocatepetl, Nevado de Toluca, and Jocotitlán stratovolcanoes and monogenetic scoria cones in the Sierra Chichinautzin Volcanic Field., 2006.
- Siebe, C., Abrams, M., Macías, J. L. and Obenholzner, J.: Repeated volcanic disasters in Prehispanic time at Popocatepetl,
500 central Mexico: Past key to the future?, *Geology*, 24(5), 399–402, doi:10.1130/0091-7613(1996)024<0399:RVDIPT>2.3.CO;2, 1996.
- Siebe, C., Salinas, S., Arana-Salinas, L., Macías, J. L., Gardner, J. and Bonasia, R.: The ~ 23,500 y 14 C BP White Pumice Plinian eruption and associated debris avalanche and Tochimilco lava flow of Popocatepetl volcano, México, *J. Volcanol. Geotherm. Res.*, 333–334, 66–95, doi:10.1016/j.jvolgeores.2017.01.011, 2017.
- 505 Siebert, L.: Landslides resulting from structural failure of volcanoes, *Rev. Eng. Geol.*, 15, 209–235, doi:10.1130/REG15-p209, 2002.
- Singh, A.: Review article digital change detection techniques using remotely-sensed data, *Int. J. Remote Sens.*, 10(6), 689–1003, doi:10.1007/BF02197115, 1989.
- Singh, S. K., Reinoso, E., Arroyo, D., Ordaz, M., Cruz-Atienza, V., Pérez-Campos, X., Iglesias, A. and Hjörleifsdóttir, V.:
510 Deadly Intraslab Mexico Earthquake of 19 September 2017 (Mw 7.1): Ground Motion and Damage Pattern in Mexico City, *Seismol. Res. Lett.*, 89(6), 2193–2203, doi:10.1785/0220180159, 2018.
- Tanarro, L. M., Andrés, N., Zamorano, J. J., Palacios, D. and Renschler, C. S.: Geomorphological evolution of a fluvial channel after primary lahar deposition: Huiloac Gorge, Popocatepetl volcano (Mexico), *Geomorphology*, 122(1–2), 178–190, doi:10.1016/j.geomorph.2010.06.013, 2010.
- 515 Vázquez-Selem, L. and Heine, K.: Late Quaternary Glaciation in Mexico, in *Developments in Quaternary Science*, vol. 15,

pp. 849–861., 2011.

Wang, F., Fan, X., Yunus, A. P., Siva Subramanian, S., Alonso-Rodriguez, A., Dai, L., Xu, Q. and Huang, R.: Coseismic landslides triggered by the 2018 Hokkaido, Japan (Mw 6.6), earthquake: spatial distribution, controlling factors, and possible failure mechanism, *Landslides*, 16(8), 1551–1566, doi:10.1007/s10346-019-01187-7, 2019.

520